Regular Article

Prospective impact of healthcare facilities and infrastructure on infectious disease outbreak dynamics: a modeling study

Jyoti Maurya[1,a], Konstantin B. Blyuss[2,b], and A. K. Misra[3,c]

[1] Department of Applied Sciences and Humanities, Invertis University, Bareilly, Uttar Pradesh 243123, India
[2] Department of Mathematics, University of Sussex, Falmer, Brighton BN1 9QH, UK
[3] Department of Mathematics, Institute of Science, Banaras Hindu University, Varanasi, Uttar Pradesh 221005, India

Abstract In epidemic outbreak control management, the synergy between healthcare facilities and infrastructure, including road networks and ambulance services, plays a pivotal role. In this article, we formulate and analyze a mathematical model that underscores the significance of infrastructure components along with healthcare facilities to effectively control an epidemic outbreak. By intricately examining the interplay between healthcare accessibility and the swift movement of medical resources, this study contributes valuable insights into optimizing response strategies during such outbreaks. Through qualitative analysis, we establish the model's susceptibility to a range of bifurcations, including transcritical (forward and backward), saddle-node, Hopf, and codimension-2 Bogdanov–Takens bifurcations. Furthermore, we provide an epidemiological interpretation of the intricate dynamic behaviors observed in the context of disease endemism. The proposed model offers insights that can guide policymakers, healthcare administrators, and urban planners in devising effective strategies for combating epidemic outbreaks while fostering community resilience.

1 Introduction

In an increasingly interconnected world, the threat posed by epidemic outbreaks to global public health has become a matter of heightened concern [19–22, 24, 28]. The emergence of new and highly contagious pathogens has underscored the urgency of addressing these global health threats. These outbreaks not only have immediate health consequences but also significant economic, social, and political impacts. They disrupt healthcare systems, strain resources, and can lead to widespread panic and social unrest. The continual emergence of these infectious diseases prompts the recognition that to control the outbreaks requires a holistic approach to managing healthcare resources and logistical infrastructure. The timely and coordinated deployment of medical resources, coupled with the efficient movement of patients, can profoundly shape the outcome of an outbreak [36].

Healthcare facilities, ranging from local clinics to specialized hospitals, constitute the frontline defense against infectious diseases. These facilities not only provide vital medical care but also act as points of containment and treatment. However, the efficacy of these medical facilities is deeply entwined with the availability and accessibility of supporting infrastructure. Efficient transportation networks, including road systems and ambulance services, ensure the rapid transfer of patients to appropriate facilities, which facilitate the distribution of medical supplies, and enable the seamless movement of healthcare personnel [13]. The shortage of ambulances can present a daunting challenge within healthcare system, with far-reaching implications for patient care and epidemic control. This inadequacy can lead to obstacles in ensuring the prompt transportation of patients to hospitals, impeding not only the prompt initiation of treatment but also the crucial isolation measures necessary during epidemics. The difficulties are made even more acute when the road networks are disrupted or inadequate, which prolongs the

[a] e-mails: jyoti92maurya@gmail.com; jyoti.m@invertis.org
[b] e-mail: k.blyuss@sussex.ac.uk
[c] e-mail: akmisra_knp@yahoo.com (corresponding author)

travel times between affected regions and medical facilities. Particularly in areas with underdeveloped or disturbed road networks, rapid access to hospitals for affected populations becomes a formidable obstacle. This, in turn, can result in elevated transmission rates and logistical complications in delivering vital medical supplies and personnel to affected areas.

The integration of mathematical modeling techniques with epidemiological insights has revolutionized our capacity to grasp the intricate dynamics of disease transmission [2, 3, 5, 6, 9, 10, 14, 18, 23, 25, 27, 29, 37, 39, 40, 42–44]. This interdisciplinary approach has proven potent in deciphering the complex web of interactions among disease spread and healthcare capabilities [4, 8, 11, 15–17, 26, 30–35, 41, 46, 47]. Wang et al. [46] proposed a Filippov epidemic model to examine the impact of healthcare capacity and limited public health resources on epidemic control. Their findings indicate that enhancing basic medical conditions, such as increasing the minimum treatment ratio, or augmenting medical resource inputs, such as hospital bed-population ratio (HBPR) and the potential maximum treatment ratio, can effectively maintain case numbers at relatively low levels when the basic reproduction number is greater than unity. Furthermore, if basic reproduction number is less than unity, these strategies can aid in eradicating the disease, though complete eradication is not always achievable due to the presence of backward bifurcation in the system. Liu et al. [27] proposed a compartmental model to illustrate a possible mechanism for multiple outbreaks or sustained periodic oscillations of emerging infectious diseases due to the psychological impact of the reported number of infectious and hospitalized individuals. Zhou and Fan [48] studied an SIR epidemic model to demonstrate the impact of limited medical resources on the transmission dynamics of infectious diseases. Their research indicates that the availability and supply efficiency of medical resources significantly influence the control of infectious diseases. Abdelrazec et al. [1] proposed a deterministic model to study the transmission dynamics of dengue fever and the influence of healthcare resources on its spread and control. They concluded that understanding disease transmission dynamics requires more than just the basic reproduction number; other epidemiological parameters, such as HBPR, also significantly impact disease transmission dynamics. Although all these works are related to healthcare facilities, they either lack the consideration of a separate class for hospitalized individuals or overlook the limitation of hospital bed availability. Addressing these gaps, this research article explores the critical connection between healthcare facilities and infrastructure in the context of epidemic outbreak management. By examining the synergies and dependencies within this triad, our study aims to contribute to the ongoing discourse on control strategies involving healthcare facilities and infrastructure. Through the lens of mathematical rigor and epidemiological depth, we seek to enrich the toolkit available to public health professionals and policymakers striving to safeguard global health in the face of emerging infectious threats. The inclusion of a hospitalized class in our mathematical model indeed introduces a novel dimension to traditional infectious disease models, such as SIR and SEIR. By incorporating a specific class for hospitalized individuals, our model offers several advantages over existing models. Firstly, it allows for a more nuanced understanding of disease dynamics by accounting for the impact of hospitalization on disease transmission and progression. Secondly, it enables us to assess healthcare system capacity and resource allocation more accurately by modeling the flow of individuals between different epidemiological states, including hospitalization. Thirdly, the hospitalized class facilitates the evaluation of interventions aimed at reducing hospitalization rates and improving patient outcomes, thus offering valuable insights for public health policy and decision-making. Overall, the addition of a hospitalized class enhances the comprehensiveness and applicability of our model in addressing real-world infectious disease scenarios. This study holds significant importance as it sheds light on how the infrastructure and functioning of healthcare systems influence the spread and control of infectious diseases. By understanding the dynamics and vulnerabilities within healthcare infrastructure, we can better anticipate and respond to outbreaks, ultimately saving lives and mitigating the impact on public health. Additionally, the exploration of bifurcations in the model provides insights into the potential tipping points or critical thresholds where interventions may have the most significant impact in containing or preventing outbreaks.

2 The mathematical model

Here, we introduce a nonlinear epidemic model that incorporates two essential factors: the availability of healthcare facilities, particularly count of hospital beds, and the infrastructure of the considered region, including ambulances and roads. The primary aim of this model is to demonstrate how the capacity of healthcare facilities and the efficiency of infrastructure can significantly impact the future course of an epidemic. Specifically, we focus on those diseases that spread through sustained human-to-human interactions, i.e., direct contact. The occurrence of these diseases sharply increases the number of individuals requiring medical attention, which can overwhelm healthcare facilities. Thus, having enough hospital beds becomes crucial for effectively managing these outbreaks. With an adequate bed capacity, hospitals can provide timely medical attention, closely monitor patients, and implement necessary isolation measures. Thus, the state of infection and hospitalization of infected individuals divides the whole population into three classes: susceptible class 'S' (includes those individuals who have not yet been infected but are at risk of acquiring the infection), infected class 'I' (includes those individuals who have tested positive

for the infectious disease, can transmit it to susceptible individuals, and have not yet received hospital beds but are seeking for better treatment) and hospitalized class 'H' (relates to individuals from the infected population who have been admitted to hospitals. Because they are hospitalized, they are effectively isolated from the general population, making them unable to spread the disease to people who have not yet been infected). Here, H_a denotes the cumulative count of hospital beds in the considered region, which is treated as a constant; thus, $(H_a - H(t)) \geq 0$ represents the count of available hospital beds at time 't'.

Moreover, a well-developed infrastructure, including roads and ambulances are also very crucial to control the outbreak. Smooth transportation and quick ambulance services ensure that patients can reach hospitals promptly for medical attention. Without these critical components, healthcare systems may struggle to cope with the sudden influx of patients, leading to compromised care and hampering efforts to control the epidemic effectively. Thus, we consider the hospital occupancy rate as a function that depends on both the infrastructure capacity and the count of infected individuals. To represent this relationship, we adopt the Holling type-II functional response [7], i.e.,

$$k(I) = k_0 + \frac{k_1 I}{m + I}.$$

The Holling Type II functional response for hospitalization rate offers a more nuanced depiction of the relationship between the number of infected individuals and hospitalization. This model recognizes the inherent non-linear dynamics play, which better mirrors the real-world scenario in epidemiology. As the number of infected individuals escalates, the rate at which people require hospitalization may indeed surge rapidly at first. This initial spike occurs as the contagion spreads and more individuals become symptomatic, necessitating medical attention. However, the Holling Type II model acknowledges that this steep incline doesn't continue indefinitely. Instead, as the influx of patients inundates healthcare systems and infrastructure, such as ambulance services, there comes a critical point where the capacity to accommodate new hospitalizations becomes constrained. At this juncture, the rate of hospitalizations begins to level off, approaching a plateau. This leveling reflects the saturation of healthcare resources, where the ability to admit additional patients becomes increasingly limited. Here, function $k(I)$ adheres the subsequent properties.

(i) $k(I) > 0$ for $I \geq 0$ and $k(0) = k_0 > 0$. This scenario reflects the situation, where the healthcare infrastructure is fixed and cannot be increased due to financial constraints or other limitations. Despite these constraints, there is still available infrastructure to accommodate a certain number of infected individuals in hospitals; thus, k_0 represents the minimum hospital occupancy rate.

(ii) $\dfrac{\partial k(I)}{\partial I} = \dfrac{mk_1}{(m + I)^2} > 0$ and $\lim_{I \to \infty} k(I) = k_0 + k_1$. Since $k(I)$ is the increasing function of I, therefore if the number of infected individuals becomes large, the rate of hospital occupancy increases and eventually reaches a plateau, reflecting the limitations of the healthcare infrastructure. Thus, k_1 represents the maximum increment in hospital occupancy rate and $(k_0 + k_1)$ is the maximum possible hospital occupancy rate.

(iii) For $I = m$, $k(I) = k_0 + \dfrac{k_1}{2}$, which represents the scenario when the increment in hospital occupancy rate is half of its maximum possible value.

Under the aforementioned assumptions, the mathematical description of the dynamics of an epidemic outbreak can be represented by the subsequent system of nonlinear ordinary differential equations.

$$\begin{cases} \dfrac{dS}{dt} = A - \beta SI - dS + \nu I + \nu_1 H, \\[2mm] \dfrac{dI}{dt} = \beta SI - (d + \alpha + \nu)I - k(I)(H_a - H)I, \\[2mm] \dfrac{dH}{dt} = k(I)(H_a - H)I - (\nu_1 + \theta\alpha + d)H, \end{cases} \tag{1}$$

where $S(0) > 0$, $I(0) \geq 0$, and $H(0) \geq 0$. Here, A denotes the immigration rate of individuals into the susceptible population, while β signifies the rate of disease transmission from infected individuals I to susceptible individuals S. The parameters ν and ν_1 denote the rates of self-recovery and hospital recovery, respectively, for infected individuals. Additionally, the proportionality constants d and α represent natural mortality and disease-induced mortality, respectively. We assume a severe infectious disease scenario where some hospitalized individuals may succumb to mortality due to the disease despite being hospitalized. Hence, θ represents the extra mortality constant of hospitalized individuals. The schematic representation of the model system (1) is depicted in Fig. 1.

Fig. 1 The schematic diagram for model system (1)
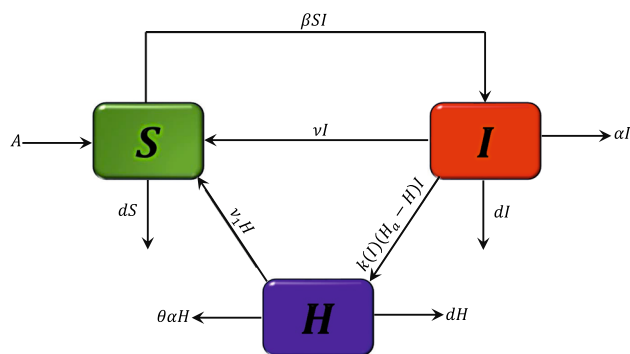
3 Basic properties

In this section, we discuss the feasibility of equilibrium for model system (1). Further, we conduct the stability analysis of these obtained equilibria. The stability analysis allows us to discern, whether the equilibrium is an attractor or repeller, and how the system responds to small perturbations.

3.1 Model equilibrium and basic reproduction number

In the absence of disease, the proposed model system (1) demonstrates a sole equilibrium denoted as $E_0\left(\frac{A}{d}, 0, 0\right)$. Consequently, we employ the next-generation matrix method [45] for determining the basic reproduction number (R_0), i.e.,

$$R_0 = \frac{\beta A}{d(d + \alpha + \nu + k_0 H_a)}.$$

Further, equilibrium $E^*(S^*, I^*, H^*)$ can be obtained by solving the subsequent algebraic equations

$$A - \beta S I - dS + \nu I + \nu_1 H = 0, \tag{2}$$

$$\beta S - (d + \alpha + \nu) - k(I)(H_a - H) = 0, \tag{3}$$

$$k(I)(H_a - H)I - (\nu_1 + \theta\alpha + d)H = 0. \tag{4}$$

From equation (4), it is apparent that (i) if $I = 0$, we have $H = 0$, (ii) $H = H_a$ is an asymptote, and (iii) $\dfrac{\partial H}{\partial I} > 0$ in the positive quadrant.

Further, using $S = \dfrac{[d + \alpha + \nu + k(I)(H_a - H)]}{\beta}$ from equation (3) in equation (2), we obtain another equation in I and H, i.e.,

$$A - [d + \alpha + k(I)(H_a - H)]I - \frac{d}{\beta}[d + \alpha + \nu + k(I)(H_a - H)] + \nu_1 H = 0. \tag{5}$$

From equation (5) it is apparent that (i) $H = H_a + \frac{d+\alpha}{k_0+k_1}$ is an asymptote, (ii) $\frac{\partial H}{\partial I} > 0$ in the positive quadrant, and (iii) for $I = 0$, we have $H = -\frac{d(R_0-1)(d+\alpha+\nu+k_0 H_a)}{dk_0+\beta\nu_1} = H_e$(say). Moreover, if we set $H = 0$, equation (5) gives the following quadratic equation in I.

$$\mathcal{A}_1 I^2 + \mathcal{A}_2 I - \mathcal{A}_3 = 0, \tag{6}$$

where

$$\mathcal{A}_1 = \beta(d + \alpha + k_0 H_a + k_1 H_a), \ \mathcal{A}_2 = \beta m(d + \alpha + k_0 H_a) + dk_1 H_a - d(R_0 - 1)(d + \alpha + \nu + k_0 H_a),$$
$$\mathcal{A}_3 = md(R_0 - 1)(d + \alpha + \nu + k_0 H_a).$$

Here, $\mathcal{A}_1$ is always positive and $\mathcal{A}_3$ can be positive, negative, or zero depending on the value of R_0. Thus, we analyze the feasibility equilibrium E^* in three scenarios, i.e., $R_0 > 1$, $R_0 = 1$, $R_0 < 1$. Thus,

(a) For $R_0 > 1$, $H_e < 0$ and equation (6) has one positive and one negative roots. Thus, isoclines (4) and (5), may intersect either at one, two, or three points, Fig. 2.
(b) For $R_0 = 1$, $H_e = 0$ and equation (6) exhibits one zero root and one negative root. Thus, isoclines (4) and (5) may intersect at one, two, or no points, Fig. 3.
(c) For $R_0 < 1$, $H_e > 0$ and equation (6) has no positive root. Thus, isoclines (4) and (5) either intersect at one point, two points or no point, Fig. 4.

Thus, based on the aforementioned analysis, we establish the following theorem concerning the existence of equilibrium for model system (1).

Theorem 1 The model system (1) has

(i) a disease-free equilibrium $E_0\left(\frac{A}{d}, 0, 0\right)$, which always exists,
(ii) one, two, or three endemic equilibria for $R_0 > 1$,
(iii) one, two, or no endemic equilibria for $R_0 \leq 1$.

3.2 Local stability analysis

Within this subsection, we provide the local stability analysis of obtained equilibria. Now, the Jacobian matrix for model system (1) can be written as

$$J = \begin{bmatrix} -(\beta I + d) & -(\beta S - \nu) & \nu_1 \\ \beta I & a_{22} & k(I)I \\ 0 & a_{32} & -(\nu_1 + \theta\alpha + d + k(I)I) \end{bmatrix},$$

where $a_{22} = \beta S - (d + \alpha + \nu) - k(I)(H_a - H) - k'(I)(H_a - H)I$, and $a_{32} = [k(I) + k'(I)I](H_a - H)$.

The eigenvalues of matrix J_0 (J evaluated at E_0) are obtained as $-d$, $-(\nu_1 + \theta\alpha + d)$, and $(R_0 - 1)(d + \alpha + \nu + k_0 H_a)$. The eigenvalue $(R_0 - 1)(d + \alpha + \nu + k_0 H_a)$ is negative for $R_0 < 1$ and positive for $R_0 > 1$, which implies equilibrium E_0 is locally asymptotically stable for $R_0 < 1$ and unstable for $R_0 > 1$.

Further, at equilibrium $E^*(S^*, I^*, H^*)$, the Jacobian matrix J can be written as

$$J^* = \begin{bmatrix} -(\beta I^* + d) & -(\beta S^* - \nu) & \nu_1 \\ \beta I^* & -k'(I^*)(H_a - H^*)I^* & k(I^*)I^* \\ 0 & a_{32}^* & -(\nu_1 + \theta\alpha + d + k(I^*)I^*) \end{bmatrix}.$$

Here, $a_{32}^* = [k(I^*) + k'(I^*)I^*](H_a - H^*)$. The characteristic equation of matrix J^* is obtained as

$$\Phi^3 + \mathcal{B}_1\Phi^2 + \mathcal{B}_2\Phi + \mathcal{B}_3 = 0, \tag{7}$$

where

$$\mathcal{B}_1 = \nu_1 + \theta\alpha + 2d + \beta I^* + k(I^*)I^* + k'(I^*)(H_a - H^*)I^*,$$
$$\mathcal{B}_2 = (\beta I^* + d)[\nu_1 + \theta\alpha + d + k(I^*)I^* + k'(I^*)(H_a - H^*)I^*] + (\nu_1 + \theta\alpha + d)k'(I^*)(H_a - H^*)I^*$$
$$\quad + \beta I^*(\beta S^* - \nu) - (k(I^*))^2(H_a - H^*)I^*,$$
$$\mathcal{B}_3 = \beta I^*[(d + \theta\alpha)k'(I^*)(H_a - H^*)I^*$$
$$\quad + (d + \alpha)(\nu_1 + \theta\alpha + d + k(I^*)I^*)$$
$$\quad + (d + \theta\alpha)k(I^*)(H_a - H^*)] + d(H_a - H^*)I^*[(\nu_1 + \theta\alpha + d)k'(I^*) - (k(I^*))^2].$$

It is evident that $\mathcal{B}_1$ is consistently positive. Applying the Routh-Hurwitz criterion, we conclude that if $\mathcal{B}_3 > 0$ and $(\mathcal{B}_1\mathcal{B}_2 - \mathcal{B}_3) > 0$, then all the eigenvalues of matrix J^* are either negative or possess negative real parts. Consequently, we state the following theorem.

Theorem 2 For model system (1)

(i)   the equilibrium E_0 demonstrates instability when $R_0 > 1$ and stability when $R_0 < 1$.
(ii) the stability of the equilibrium E^* is guaranteed when $\mathcal{B}_3 > 0$ and $(\mathcal{B}_1\mathcal{B}_2 - \mathcal{B}_3) > 0$

4 Bifurcation analysis

Here, we delve into a comprehensive analysis of the conditions that result in various bifurcation phenomena in the context of model system (1). Our particular focus centers on two critical parameters, namely the count of hospital beds H_a and the hospital occupancy rate $k(I)$. These parameters hold substantial biological significance and directly influence the dynamics of epidemic outbreaks.

4.1 Transcritical bifurcation

In this subsection, we employ the center manifold theorem [12] to determine the condition under which transcritical bifurcation occurs. From Theorem 2, it is found that there is a shift in the stability characteristics of equilibrium E_0 at the critical value $R_0 = 1$. Thus, at this critical threshold, one of the eigenvalues of matrix J_0 becomes zero, resulting in the transformation of equilibrium point E_0 into a non-hyperbolic equilibrium, and $R_0 = 1$ corresponds to $\beta = \beta^* = d(d + \alpha + \nu + k_0 H_a)/A$. Now, we introduce $S = z_1$, $I = z_2$ and $H = z_3$; consequently, the model system described by equation (1) can be expressed as

$$
\begin{cases}
\dfrac{dz_1}{dt} = A - \beta z_1 z_2 - dz_1 + \nu z_2 + \nu_1 z_3 := f_1, \\[2mm]
\dfrac{dz_2}{dt} = \beta z_1 z_2 - (d + \alpha + \nu) z_2 - k(z_2)(H_a - z_3) z_2 := f_2, \\[2mm]
\dfrac{dz_3}{dt} = k(z_2)(H_a - z_3) z_2 - (\nu_1 + \theta\alpha + d) z_3 := f_3,
\end{cases}
\tag{8}
$$

where $k(z_2) = k_0 + \dfrac{k_1 z_2}{m + z_2}$.

Moreover, the linearized matrix of system (8) when evaluated at E_0 and $\beta = \beta^*$ can be written as

$$
J_0|_{(\beta = \beta^*)} = \begin{bmatrix} -d & -\left(\frac{\beta^* A}{d} - \nu\right) & \nu_1 \\ 0 & 0 & 0 \\ 0 & k_0 H_a & -(\nu_1 + \theta\alpha + d) \end{bmatrix}.
\tag{9}
$$

The right and left eigenvectors corresponding to the eigenvalue 0 are $\tilde{\mathcal{U}} = [\tilde{u}_1 \; \tilde{u}_2 \; \tilde{u}_3]^\top$ and $\tilde{\mathcal{V}} = [\tilde{v}_1 \; \tilde{v}_2 \; \tilde{v}_3]$, respectively, where

$$
\tilde{u}_1 = -\left(\frac{\beta^* A}{d} - \nu\right)(\nu_1 + \theta\alpha + d) + \nu_1 k_0 H_a, \;\; \tilde{u}_2 = d(\nu_1 + \theta\alpha + d), \; \tilde{u}_3 = dk_0 H_a,
$$
$$
\tilde{v}_1 = 0, \;\; \tilde{v}_2 = 1, \;\; \tilde{v}_3 = 0.
$$

Thus, for model system (1) the coefficients a and b described in Theorem 4.1 of [12] can be written as

$$
a = \sum_{k,\,i,\,j=1}^{3} \tilde{v}_k \tilde{u}_i \tilde{u}_j \frac{\partial^2 f_k}{\partial z_i \partial z_j}(E_0, \beta^*), \;\; \text{and} \;\; b = \sum_{k,\,i=1}^{3} \tilde{v}_k \tilde{u}_i \frac{\partial^2 f_k}{\partial z_i \partial \beta}(E_0, \beta^*).
$$

Here,

$$
a = 2d(\nu_1 + \theta\alpha + d)\left[\beta^*\left(-\left(\frac{\beta^* A}{d} - \nu\right)(\nu_1 + \theta\alpha + d) + \nu_1 k_0 H_a\right) + dk_0^2 H_a - \frac{dk_1 H_a(\nu_1 + \theta\alpha + d)}{m}\right],
$$
$$
b = A(\nu_1 + \theta\alpha + d).
$$

Here, the parameter b is invariably positive, while a can be a positive value or negative value contingent on the parameter values. Consequently, we synthesize the observations regarding the existence of the transcritical bifurcation within the framework of the ensuing theorem.

Theorem 3 The model system (1) exhibits a transcritical bifurcation at $R_0 = 1$ (or $\beta = \beta^*$) in the forward direction if $a < 0$. Conversely, the direction of the transcritical bifurcation shifts to the backward direction if $a > 0$.

Remark 1 If $a < 0$, the forward transcritical bifurcation occur and it signifies that disease will always persist in the population if the basic reproduction number is greater than one and dies when $R_0 < 1$. On the other hand, if $a > 0$, the backward transcritical bifurcation occurs and in this case the disease may persist in the population even if the basic reproduction number is less than unity.

4.2 Saddle-node bifurcation

From Theorem 1, it is evident that model system (1) may exhibit two or three endemic equilibria depending on the parameter values. Consequently, there may be a chance that model system (1) undergoes a saddle-node bifurcation. The saddle-node bifurcation is characterized by a local phenomenon where two equilibrium points of a dynamical system come into proximity and cease to exist as they mutually annihilate each other. To explore the condition under which model system (1) exhibits saddle-node bifurcation, we utilize the Sotomayor's theorem [38]. To achieve this, we assume that there exists a critical value of $\beta = \beta_c$, which gives $\mathcal{B}_3(\beta_c) = 0$. Subsequently, matrix J^* has a zero eigenvalue. Suppose that $\hat{\mathcal{U}} = [\hat{u}_1 \ \hat{u}_2 \ \hat{u}_3]^\top$ and $\hat{\mathcal{W}} = [\hat{w}_1 \ \hat{w}_2 \ \hat{w}_3]$, represent the right and left eigenvectors of matrix J^* corresponding to the 0 eigenvalue, where

$$\hat{u}_1 = \left[k'(I^*)(\nu_1 + \theta\alpha + d) - (k(I^*))^2 \right](H_a - H^*),$$
$$\hat{u}_2 = \beta_c[\nu_1 + \theta\alpha + d + k(I^*)I^*],$$
$$\hat{u}_3 = \beta_c[k(I^*)(H_a - H^*) + k'(I^*)(H_a - H^*)I^*],$$
$$\hat{w}_1 = \beta_c I^*[\nu_1 + \theta\alpha + d + k(I^*)I^*],$$
$$\hat{w}_2 = (\beta_c I^* + d)[\nu_1 + \theta\alpha + d + k(I^*)I^*], \quad \hat{w}_3 = \nu_1\beta_c I^* + (\beta_c I^* + d)k(I^*)I^*.$$

Suppose $\hat{G} = [\hat{g}_1, \hat{g}_2, \hat{g}_3]$, where $\hat{g}_1$, $\hat{g}_2$ and $\hat{g}_3$ are right-hand sides of dS/dt, dI/dt and dH/dt, respectively, in model system (1). Then,

$$\mathcal{B}_1 = \hat{\mathcal{W}} \cdot \frac{\partial\hat{G}}{\partial\beta}\bigg|_{(E^*, \beta_c)} = d[\nu_1 + \theta\alpha + d + k(I^*)I^*]S^*I^*,$$

and

$$\mathcal{B}_2 = \hat{\mathcal{W}}\left[D^2\hat{G}(\hat{\mathcal{U}}, \hat{\mathcal{U}}) \right]\bigg|_{(E^*, \beta_c)}$$
$$= 2\beta_c\hat{u}_1\hat{u}_2(\hat{w}_3 - \hat{w}_1) + [2k'(I^*)\hat{u}_3 - k''(I^*)(H_a - H^*)I^*\hat{u}_2](\hat{w}_2 - \hat{w}_3)\hat{u}_2.$$

Here, the conditions stipulated by Sotomayor's theorem for the occurrence of a saddle-node bifurcation are satisfied whenever $\mathcal{B}_2 \neq 0$. Consequently, we state the following theorem concerning the existence of a saddle-node bifurcation.

Theorem 4 If $\beta = \beta_c$, such that $\mathcal{B}_2 \neq 0$, then model system (1) exhibits saddle-node bifurcation at equilibrium E^*.

Remark 2 The occurrence of saddle-node bifurcation holds significant biological importance as it marks a critical threshold in the dynamics of disease spread. For parameter β, i.e., transmission rate below the quantity β_c, the disease dies out quickly or attains the lowest equilibrium level due to insufficient transmission, while above it, the infection can spread exponentially, potentially leading to an epidemic outbreak. This bifurcation serves as a tipping point, delineating the boundary between disease eradication and epidemic propagation.

4.3 Hopf bifurcation

In this subsection, our objective is to explore the conditions leading to Hopf bifurcation [35] in the model system (1) at E^*. For this analysis, we assign the parameter β as the bifurcation parameter. We identify a critical value for β denoted as β_r for which $\mathcal{B}_1(\beta_r)\mathcal{B}_2(\beta_r) - \mathcal{B}_3(\beta_r) = 0$ holds. Consequently, for $\beta = \beta_r$, the equation (7) can be expressed as follows

$$(\Phi + \mathcal{B}_1)(\Phi^2 + \mathcal{B}_2) = 0.$$

The above equation yields three roots: $\Phi_{1,2} = \pm i\omega$ and $\Phi_3 = \xi$, where $\omega = \sqrt{\mathcal{B}_2}$ and $\xi = -\mathcal{B}_1$. To demonstrate the transversality condition, let's consider any point within ϵ-neighborhood of β_r, which results in $\Phi_{1,2} = \varrho(\beta)\pm i\omega(\beta)$. Substituting this into equation (7) and computing the real and imaginary components, we obtain

$$\varrho^3 - 3\varrho\omega^2 + \mathcal{B}_1(\varrho^2 - \omega^2) + \mathcal{B}_2\varrho + \mathcal{B}_3 = 0, \tag{10}$$

$$3\varrho^2\omega - \omega^3 + 2\mathcal{B}_1\varrho\omega + \mathcal{B}_2\omega = 0. \tag{11}$$

As $\omega(\beta) \neq 0$, from equation (11), we have

$$\omega^2 = 3\varrho^2 + 2\mathcal{B}_1\varrho + \mathcal{B}_2.$$

Substituting this in equation (10), we have

$$8\varrho^3 + 8\mathcal{B}_1\varrho^2 + 2\varrho(\mathcal{B}_1^2 + \mathcal{B}_2) + (\mathcal{B}_1\mathcal{B}_2 - \mathcal{B}_3) = 0. \tag{12}$$

From equation (12), we get

$$\left.\frac{d\varrho}{d\beta}\right|_{\beta=\beta_r} = -\left[\frac{1}{2(\mathcal{B}_1^2 + \mathcal{B}_2)}\frac{d}{d\beta}(\mathcal{B}_1\mathcal{B}_2 - \mathcal{B}_3)\right]_{\beta=\beta_r} \neq 0,$$

$$\text{provided } \left[\frac{d}{d\beta}(\mathcal{B}_1\mathcal{B}_2 - \mathcal{B}_3)\right]_{\beta=\beta_r} \neq 0.$$

Therefore, summing up the above results, we have

Theorem 5 For Hopf-bifurcation to occur around equilibrium E^*, the necessary and sufficient condition is that there exists a critical value of β, denoted as β_r, such that

(i) $\mathcal{B}_1(\beta_r)\mathcal{B}_2(\beta_r) - \mathcal{B}_3(\beta_r) = 0,$

(ii) $\left[\dfrac{d}{d\beta}(\mathcal{B}_1\mathcal{B}_2 - \mathcal{B}_3)\right]_{(E^*,\beta_r)} \neq 0$.

Remark 3 Hopf bifurcation signifies the transition from stable (or unstable) equilibrium to sustained oscillations or periodic outbreaks when the transmission rate β crosses the threshold quantity β_r. The biological significance of Hopf bifurcation lies in its ability to predict the emergence of sustained oscillations in the number of infected individuals over time, indicating the potential for recurring epidemic waves. This transition is crucial for understanding the long-term behavior of infectious diseases.

4.3.1 Bogdanov–Takens bifurcation

From the stability analysis of equilibrium E^*, it becomes apparent that for some $\beta = \beta_k$ and $H_a = H_{ak}$ if $\mathcal{B}_2(\beta_k, H_{ak}) = \mathcal{B}_3(\beta_k, H_{ak}) = 0$, then equation (7) possesses an eigenvalue 0, with algebraic multiplicity 2. This scenario signifies the possibility of a Bogdanov-Takens bifurcation occurring around the endemic equilibrium E^* [41]. Consequently, to investigate the existence of a Bogdanov-Takens bifurcation at equilibrium E^*, we employ the transformation $S = S^* + \tilde{x}_1$, $I = I^* + \tilde{x}_2$, and $H = H^* + \tilde{x}_3$, which shifts the equilibrium E^* to the origin.

Suppose, $\tilde{p}_1 = (\beta_k I^* + d)$, $\tilde{p}_2 = [k(I^*) + k'(I^*)I^*]$, $\tilde{p}_3 = [\nu_1 + \theta\alpha + d + k(I^*)I^*]$, and $\tilde{p}_4 = [k'(I^*) + 2k''(I^*)I^*]$. Thus, the transformation leads to the following linearized system of model system (1).

$$
\begin{bmatrix} \tilde{x}_1 \\ \tilde{x}_2 \\ \tilde{x}_3 \end{bmatrix}' = \begin{bmatrix} -\tilde{p}_1 & -(\beta_k S^* - \nu) & \nu_1 \\ \beta_k I^* - k'(I^*)(H_{ak} - H^*)I^* & k(I^*)I^* \\ 0 & \tilde{p}_2(H_{ak} - H^*) & -\tilde{p}_3 \end{bmatrix} \begin{bmatrix} \tilde{x}_1 \\ \tilde{x}_2 \\ \tilde{x}_3 \end{bmatrix} + \begin{bmatrix} -\beta_k \tilde{x}_1 \tilde{x}_2 \\ \beta_k \tilde{x}_1 \tilde{x}_2 - \tilde{p}_4 x_2^2 + \tilde{p}_2 \tilde{x}_2 \tilde{x}_3 \\ \tilde{p}_4 x_2^2 - \tilde{p}_2 \tilde{x}_2 \tilde{x}_3 \end{bmatrix}. \tag{13}
$$

Then, the generalized eigenvectors for eigenvalue $\Phi = 0$ are $\tilde{V}_1 = [\tilde{v}_{11}\ \tilde{v}_{21}\ \tilde{v}_{31}]^\top$ and $\tilde{V}_2 = [\tilde{v}_{12}\ \tilde{v}_{22}\ \tilde{v}_{32}]^\top$, which satisfy $J^*\tilde{V}_1 = 0$ and $J^*\tilde{V}_2 = \tilde{V}_1$. Here,

$$
\tilde{v}_{11} = \left[k'(I^*)(\nu_1 + \theta\alpha + d) - (k(I^*))^2 \right](H_{ak} - H^*), \ \tilde{v}_{21} = \beta_k \tilde{p}_3,
$$
$$
\tilde{v}_{31} = \beta_k \tilde{p}_2 \left(H_{ak} - H_3^* \right)],
$$
$$
\tilde{v}_{12} = \tilde{p}_3 + k'(I^*)(H_{ak} - H^*)I^*, \ \tilde{v}_{22} = \beta_k I^*, \ \ \tilde{v}_{32} = 0.
$$

Also, the eigenvector corresponding to the eigenvalue $\Phi = -[\tilde{p}_1 + k'(I^*)(H_{ak} - H^*)I^* + \tilde{p}_3]$ is $\tilde{V}_3 = [\tilde{v}_{13}\ \tilde{v}_{23}\ \tilde{v}_{33}]^\top$, where

$$
\tilde{v}_{13} = (\tilde{p}_1 + \tilde{p}_3)[\tilde{p}_1 + k'(I^*)(H_{ak} - H^*)I^*] - \tilde{p}_2 k(I^*)(H_{ak} - H^*)I^*,
$$
$$
\tilde{v}_{23} = -\beta_k[\tilde{p}_1 + k'(I^*)(H_{ak} - H^*)I^*]I^*, \ \tilde{v}_{33} = \beta_k \tilde{p}_2(H_{ak} - H^*)I^*.
$$

Let $\tilde{Q} = [\tilde{V}_1\ \tilde{V}_2\ \tilde{V}_3]$, thus by using the non-singular linear transformation, we have

$$
\begin{bmatrix} \tilde{x}_1 \\ \tilde{x}_2 \\ \tilde{x}_3 \end{bmatrix} = \tilde{Q} \begin{bmatrix} \tilde{\mathscr{Z}}_1 \\ \tilde{\mathscr{Z}}_2 \\ \tilde{\mathscr{Z}}_3 \end{bmatrix},
$$

where the inverse of matrix $\tilde{Q}$ is given as

$$
\tilde{Q}^{-1} = \begin{bmatrix} \tilde{q}_{11} & \tilde{q}_{12} & \tilde{q}_{13} \\ \tilde{q}_{21} & \tilde{q}_{22} & \tilde{q}_{23} \\ \tilde{q}_{31} & \tilde{q}_{32} & \tilde{q}_{33} \end{bmatrix}.
$$

Thus, the system (13) becomes

$$
\begin{cases} \tilde{\mathscr{Z}}_1' = \tilde{\mathscr{Z}}_2 + \tilde{L}_{20}\tilde{\mathscr{Z}}_1^2 + \tilde{L}_{11}\tilde{\mathscr{Z}}_1\tilde{\mathscr{Z}}_2 + \tilde{L}_{02}\tilde{\mathscr{Z}}_1\tilde{\mathscr{Z}}_2 + \tilde{\mathscr{Z}}_3.O\left(|\tilde{\mathscr{Z}}_1,\ \tilde{\mathscr{Z}}_2|^3\right), \\ \tilde{\mathscr{Z}}_2' = \tilde{M}_{20}\tilde{\mathscr{Z}}_1^2 + \tilde{M}_{11}\tilde{\mathscr{Z}}_1\tilde{\mathscr{Z}}_2 + \tilde{M}_{02}\tilde{\mathscr{Z}}_1\tilde{\mathscr{Z}}_2 + \tilde{\mathscr{Z}}_3.O\left(|\tilde{\mathscr{Z}}_1,\ \tilde{\mathscr{Z}}_2|^3\right), \\ \tilde{\mathscr{Z}}_3' = -[\tilde{p}_1 + k'(I^*)(H_{ak} - H^*)I^* + \tilde{p}_3]\tilde{\mathscr{Z}}_3 + O\left(|\tilde{\mathscr{X}}_1,\ \tilde{\mathscr{X}}_2|^3\right), \end{cases} \tag{14}
$$

where

$$
\tilde{L}_{20} = \beta_k \tilde{v}_{11}\tilde{v}_{21}(\tilde{q}_{12} - \tilde{q}_{11}) + \left[-\tilde{p}_4(H_{ak} - H^*)\tilde{v}_{21}^2 + \tilde{p}_2\tilde{v}_{21}\tilde{v}_{31} \right](\tilde{q}_{12} - \tilde{q}_{13}),
$$
$$
\tilde{L}_{11} = \beta_k(\tilde{v}_{11}\tilde{v}_{22} + \tilde{v}_{12}\tilde{v}_{21})(\tilde{q}_{12} - \tilde{q}_{11}) + [-2\tilde{p}_4(H_{ak} - H^*)\tilde{v}_{21}\tilde{v}_{22} + \tilde{p}_2\tilde{v}_{22}\tilde{v}_{31}](\tilde{q}_{12} - \tilde{q}_{13}),
$$
$$
\tilde{L}_{02} = \beta_k \tilde{v}_{12}\tilde{v}_{22}(\tilde{q}_{12} - \tilde{q}_{11}) - \tilde{p}_4(H_{ak} - H^*)\tilde{v}_{22}^2(\tilde{q}_{12} - \tilde{q}_{13}),
$$
$$
\tilde{M}_{20} = \beta_k \tilde{v}_{11}\tilde{v}_{21}(\tilde{q}_{22} - \tilde{q}_{21}) + \left[-\tilde{p}_4(H_{ak} - H^*)\tilde{v}_{21}^2 + \tilde{p}_2\tilde{v}_{21}\tilde{v}_{31} \right](\tilde{q}_{22} - \tilde{q}_{23}),
$$
$$
\tilde{M}_{11} = \beta_k(\tilde{v}_{11}\tilde{v}_{22} + \tilde{v}_{12}\tilde{v}_{21})(\tilde{q}_{22} - \tilde{q}_{21}) + [-2\tilde{p}_4(H_{ak} - H^*)\tilde{v}_{21}\tilde{v}_{22} + \tilde{p}_2\tilde{v}_{22}\tilde{v}_{31}](\tilde{q}_{22} - \tilde{q}_{23}),
$$
$$
\tilde{M}_{02} = \beta_k \tilde{v}_{12}\tilde{v}_{22}(\tilde{q}_{22} - \tilde{q}_{21}) - \tilde{p}_4(H_{ak} - H^*)\tilde{v}_{22}^2(\tilde{q}_{22} - \tilde{q}_{23}).
$$

Further, model system (14) possesses a center manifold, that can be locally represented as follows:

$$
W^c = \{(\tilde{\mathscr{Z}}_1,\ \tilde{\mathscr{Z}}_2,\ \tilde{\mathscr{Z}}_3) \mid \tilde{\mathscr{Z}}_3 = \tilde{F}(\tilde{\mathscr{Z}}_1,\ \tilde{\mathscr{Z}}_2),\ |\tilde{\mathscr{Z}}_1| < \tilde{\epsilon}_1,\ |\tilde{\mathscr{Z}}_2| < \tilde{\epsilon}_2,\ \ \tilde{F}(0,0) = D\tilde{F}(0,0) = 0\},
$$

for very small $\tilde{\epsilon}_1$ and $\tilde{\epsilon}_2$. Now the system (14) restricted to the center manifold is represented as

$$
\begin{cases}
\tilde{\mathscr{Z}}_1' = \tilde{\mathscr{Z}}_2 + \tilde{L}_{20}\tilde{\mathscr{Z}}_1^2 + \tilde{L}_{11}\tilde{\mathscr{Z}}_1\tilde{\mathscr{Z}}_2 + \tilde{L}_{02}\tilde{\mathscr{Z}}_2^2, \\
\tilde{\mathscr{Z}}_2' = \tilde{M}_{20}\tilde{\mathscr{Z}}_1^2 + \tilde{M}_{11}\tilde{\mathscr{Z}}_1\tilde{\mathscr{Z}}_2 + \tilde{M}_{02}\tilde{\mathscr{Z}}_2^2.
\end{cases}
\tag{15}
$$

Therefore, using the near-identity transformation,

$$
\begin{cases}
\tilde{\mathscr{Z}}_1 = \tilde{\mathscr{U}}_1 + \dfrac{1}{2}(\tilde{L}_{11} + \tilde{L}_{02})\tilde{\mathscr{U}}_1^2 + \tilde{M}_{02}\tilde{\mathscr{U}}_1\tilde{\mathscr{U}}_2, \\
\tilde{\mathscr{Z}}_2 = \tilde{\mathscr{U}}_2 - \tilde{L}_{20}\tilde{\mathscr{U}}_1^2 + \tilde{M}_{02}\tilde{\mathscr{U}}_1\tilde{\mathscr{U}}_2,
\end{cases}
\tag{16}
$$

and substituting $\tilde{\mathscr{U}}_1$, $\tilde{\mathscr{U}}_2$ into $\tilde{\mathscr{Z}}_1$, $\tilde{\mathscr{Z}}_2$, we get

$$
\begin{cases}
\tilde{\mathscr{Z}}_1' = \tilde{\mathscr{Z}}_2, \\
\tilde{\mathscr{Z}}_2' = \tilde{\mathscr{M}}_{20}\tilde{\mathscr{Z}}_1^2 + \tilde{\mathscr{M}}_{11}\tilde{\mathscr{Z}}_1\tilde{\mathscr{Z}}_2,
\end{cases}
\tag{17}
$$

where $\tilde{\mathscr{M}}_{20} = \tilde{M}_{20}$, $\tilde{\mathscr{M}}_{11} = \tilde{M}_{11} + 2\tilde{L}_{20}$ and for Bogdanov–Takens bifurcation to be non-degenerate, we consider $\tilde{\mathscr{M}}_{20} \neq 0$ and $\tilde{\mathscr{M}}_{11} \neq 0$. Thus, we have the following theorem.

Theorem 6 If there exist critical values $\beta = \beta_k$ and $H_a = H_{ak}$, such that $\tilde{\mathscr{M}}_{20} \neq 0$ and $\tilde{\mathscr{M}}_{11} \neq 0$, then model system (1) demonstrates a Bogdanov–Takens bifurcation of codimension-2 around the equilibrium E^*.

5 Numerical simulations

This section encompasses the visualization and validation of outcomes obtained in preceding sections through numerical simulations. To discuss all the obtained dynamical properties, we have chosen a set of hypothetical parameter values for simulations, which are listed in Table 1. The component of equilibrium E^* for these parameter values are obtained as

$$
S^* = 793 \text{ persons}, \quad I^* = 152 \text{ persons}, \quad H^* = 88 \text{ persons}.
$$

The eigenvalues of matrix J^* are obtained as $\Phi_{1,2} = -0.0036 \pm 0.044i$, and $\Phi_3 = -0.6095$. Here, two eigenvalues are complex conjugates with negative real parts and one eigenvalue is negative, that confirms the local stability of equilibrium E^*.

In order to comprehensively depict the dynamics inherent in model system (1), we plot three equilibrium curves in $R_0 - I$ plane, Fig. 5a. The plotted curves correspond to three distinct values of k_1, i.e., $k_1 = 0.0001$ (labeled

Table 1 Biological description and considered parameter values in model system (1)

Parameter	Description	Value
A	Immigration rate	20 persons day^{-1}
β	Transmission rate of individuals from susceptible class to infected class	0.0002 person^{-1} day^{-1}
k_0	Hospital occupancy rate	0.0005 person^{-1} day^{-1}
k_1	Maximum increment in hospital occupancy rate	0.003 person^{-1} day^{-1}
m	Half saturation constant	10 persons
ν	Self recovery rate	0.04 day^{-1}
α	Disease induced mortality rate	0.07 day^{-1}
ν_1	Hospital recovery rate	0.06 day^{-1}
H_a	Count of total hospital beds	100
d	Natural mortality rate	0.009 day^{-1}
θ	Disease related death proportionality constant of hospitalized population	0.0001

as $\boxed{1}$), $k_1 = 0.0008$ (labeled as $\boxed{2}$), and $k_1 = 0.005$ (labeled as $\boxed{3}$). This figure shows that the curves distinctly demonstrate a forward transcritical bifurcation at $R_0 = 1$ and the equilibrium level of infected individuals decreases with increasing value of k_1. Additionally, curve $\boxed{2}$ showcases the manifestation of Hopf bifurcation at two distinct points, while curve $\boxed{3}$ exhibits saddle-node bifurcation at two points and Hopf bifurcation at one point. We have plotted the coefficient a of Theorem 3 against values of k_1 within the interval (0, 0.0057) in Fig. 5b. The graph illustrates that the coefficient a consistently maintains a negative value. Consequently, for the specified range of parameter values, model system (1) consistently exhibits a transcritical bifurcation in the forward direction. We have also marked the value of a for $k_1 = 0.0001, \ 0.0008, \ 0.005$ with red color dots. To understand the dynamics exhibits by curve $\boxed{2}$ and $\boxed{3}$ in more detail, we separately plot the bifurcation diagram in Figs. 6a and b, respectively. From Fig. 6a, we can see that the equilibrium curve exhibits Hopf bifurcation at $R_0 \approx 1.318$ (first Lyapunov coefficient $(\mathcal{L}_1) = -1.055 \times 10^{-7}$) and $R_0 \approx 1.707$ ($\mathcal{L}_1 = -2.112 \times 10^{-8}$). As the first Lyapunov coefficients are negative at these Hopf points, thus both of Hopf points exhibit supercritical nature. Consequently, stable limit cycles emanate from one of the Hopf points and cease to appear at the other, which reveals that model system (1) showcases 'bubbling' phenomenon between these two points.

Biological significance of Figure 6a: For $R_0 \in (1.318, 1.707)$, the number of infected individuals exhibits fluctuations corresponding to the amplitude of the stable limit cycle. This continual oscillation in the infected population presents a significant challenge for healthcare managers and policymakers in devising effective strategies to control the prevalence of the infectious disease. The unpredictability inherent in these fluctuations impedes the implementation of consistent and sustainable intervention measures. Consequently, eradication of the disease from the population becomes a formidable task.

Further, Fig. 6b shows the bifurcation plot for the curve $\boxed{3}$. This figure illustrates that the equilibrium curve $\boxed{3}$ exhibits the emergence of two additional branches as R_0 increases. This phenomenon occurs as a result of saddle-node bifurcation, that takes place at $R_0 \approx 1.724$ and $R_0 \approx 2.058$. Among these branches, the upper two branches are unstable, while the lower one exhibits stability. Also, the equilibrium curve manifests Hopf bifurcation at $R_0 \approx 2.533$, which is subcritical in nature. Thus, from the Hopf point, two limit cycles originate from which the inner limit cycle is unstable, and the outer limit cycle is stable. These two limit cycles collide and cease to appear through limit cycle bifurcation at $R_0 \approx 2.866$. Additionally, at $R_0 \approx 2.058$, the phenomenon of homoclinic bifurcation transpires, where the stable limit cycle collides with an unstable equilibrium point, resulting in the discontinuation of the stable limit cycle's existence. Consequently, the number of infected individuals will always gravitate towards the equilibrium associated with low endemicity, which is stable or approaches to the stable limit cycle as $t \to \infty$, whenever $R_0 \in (2.529, 2.866)$. On the other hand, for $R_0 \in (2.058, 2.529)$, the solution trajectories always gravitate towards stable limit cycle.

Biological significance of Figure 6b: When $R_0 \in (1.724, 2.058)$, the infected population reaches at the equilibrium level of the lower branch of the equilibrium curve, ensuring that the disease persists in the population. For $R_0 \in (2.058, 2.529)$, the number of infected individuals fluctuates, influenced by the amplitude of the stable limit cycle. In this scenario, decision-making regarding disease eradication becomes highly complex due to the variability in the number of infected individuals. Furthermore, for $R_0 \in (2.529, 2.866)$, the number of infected individuals may either fluctuate based on the stable limit cycle's amplitude or stabilize at an equilibrium level, contingent upon the initial size of the infected population within the considered region.

Remark 4 Based on these observed dynamics, it is evident that when healthcare facilities are ample in the affected area, an increase in logistical infrastructure may actually reduce the equilibrium level of infected individuals. However, it is important to note that beyond a certain limit, further addition to the logistic infrastructures could potentially complicate the situation rather than improve it.

Further, we plot the saddle-node curve (black curve) and Hopf curve (white curve) in $R_0 - H_a$ bi-parametric plane for $k_0 = 0.0007$ and $k_1 = 0.009$ (remaining parameter values are same as mentioned in Table 1), Fig. 7. The saddle-node curve encompasses two cusp points, which are labeled by 'CP'. On the other hand, within Hopf curve, there are two instances of generalized Hopf points, denoted as 'GH', along with a Bogdanov-Takens point, marked as 'BT'. The complete parametric plane is partitioned into four discernible regions by these two curves. These regions are represented by the colors orange (Region I), purple (Region II), green (Region III), and blue (Region IV). The proposed system (1) exhibits distinct dynamical behaviors in these regions. In Region I, there exists an endemic equilibrium point that is unique for this parameter combination. Within Region II, the model system (1) displays three endemic equilibrium points, with two being unstable and one being stable. Transitioning to the Region III, an unstable endemic equilibrium point is encompassed by a stable limit cycle. Finally, within the Region IV, a stable endemic equilibrium point is enclosed by an unstable limit cycle.

We again plot three equilibrium curves for $H_a = 50$, $m = 60$, and $k_1 = 0.0001$ (the remaining parameter values are same as mentioned in Table 1), Fig. 8a. These three curves correspond to $k_0 = 0.00122$ (labeled as $\boxed{1}$), $k_0 = 0.0014$ (labeled as $\boxed{2}$), and $k_0 = 0.0024$ (labeled as $\boxed{3}$). From this figure, we can see that all the three
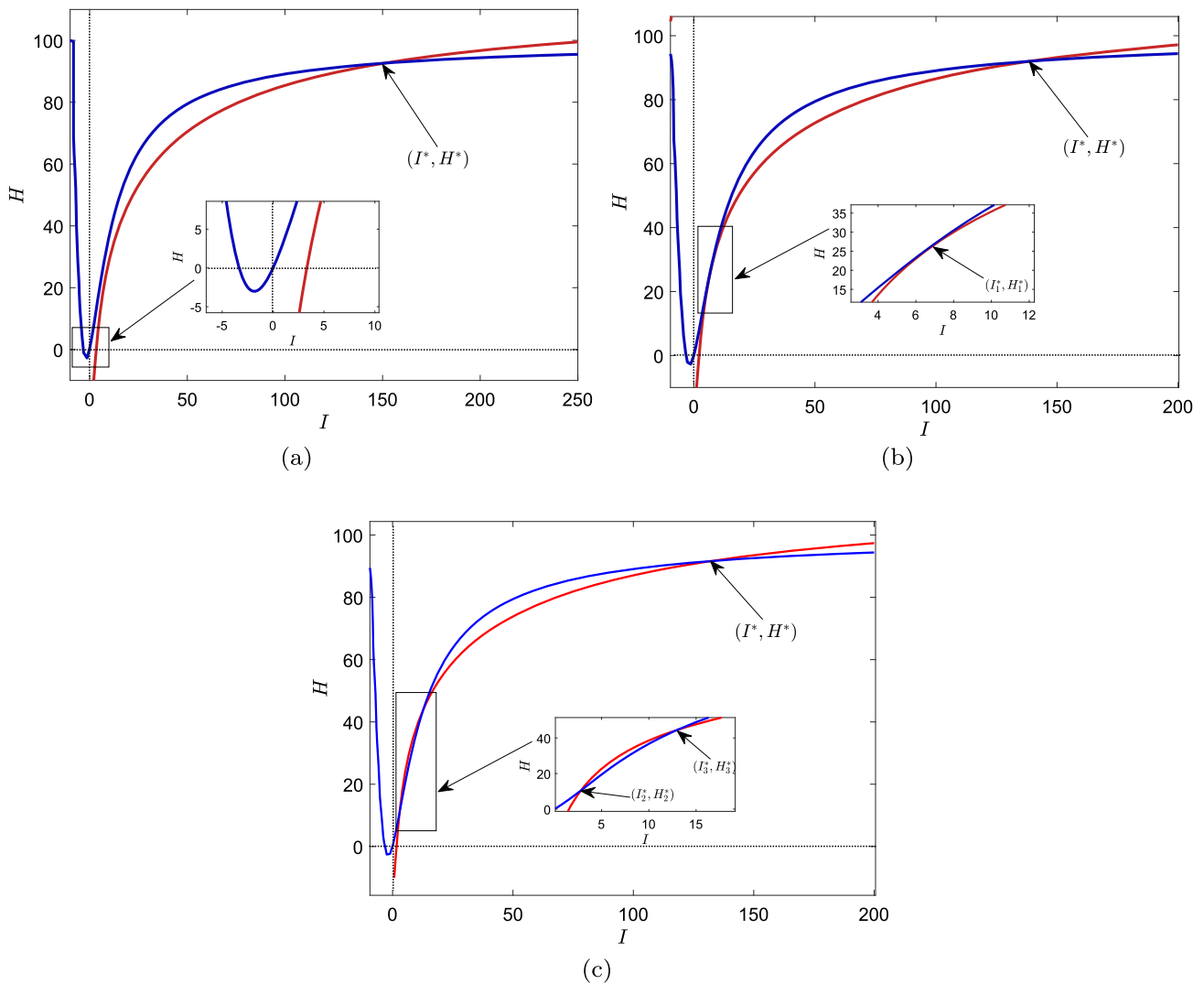
Fig. 2 (**a**–**c**) Intersection scenarios of isoclines (4) and (5) for $R_0 > 1$. Blue curve depicts isocline (4) and red curve depicts isocline (5)

curves showcase backward transcritical bifurcation at $R_0 = 1$. We further plot the coefficient a of Theorem 3, over the range $k_0 \in (0, 0.0025)$, Fig. 8b. From this plot, it becomes evident that for $k_0 > 0.0011$, a is consistently positive, while for $k_0 < 0.0011$, a takes negative values. This observation implies that when $k_0 > 0.0011$, the model system (1) invariably exhibits a transcritical bifurcation in the backward direction. This intriguing phenomenon of a backward transcritical bifurcation signifies a crucial insight. It demonstrates that the disease can endure within the population despite having R_0 less than one. This occurrence challenges the conventional understanding, suggesting that even when the conditions might seemingly not favor the disease's persistence, certain factors and dynamics come into play, allowing the disease to persist in the population. This figure also depicts that as the value of k_0 is raised, the equilibrium level of infected individuals experiences a corresponding increase. This observation emphasizes a vital understanding of how the presence and adequacy of hospital resources and infrastructure can significantly influence the dynamics of infectious disease transmission. This result suggests that if the total count of hospital beds within the affected regions remains below a certain critical threshold, the equilibrium level of infected individuals escalates, even though the basic infrastructure is well-developed and maintained. The equilibrium curves presented in Fig. 8 also contain Hopf point(s). Therefore, in order to comprehensively grasp the entire dynamics, we have plotted bifurcation diagrams in Fig. 9 for $k_0 = 0.00122$, $k_0 = 0.0014$, and $k_0 = 0.0024$. Figure 9a corresponds to the bifurcation diagram associated with $k_0 = 0.00122$. This figure shows the 'bubbling' phenomenon between two Hopf points, which occurs at $R_0 \approx 1.003$ and $R_0 \approx 1.06$. Notably, these Hopf points are characterized by their supercritical nature. Therefore, for $R_0 \in (1.003, 1.06)$, the stable branch of equilibrium curve converts into an unstable branch. Furthermore, this unstable branch envelops itself with a stable limit cycle. Also, at $R_0 = 0.995$ the equilibrium curve manifests saddle-node bifurcation. Trajectories for $R_0 \in (0.995, 1)$
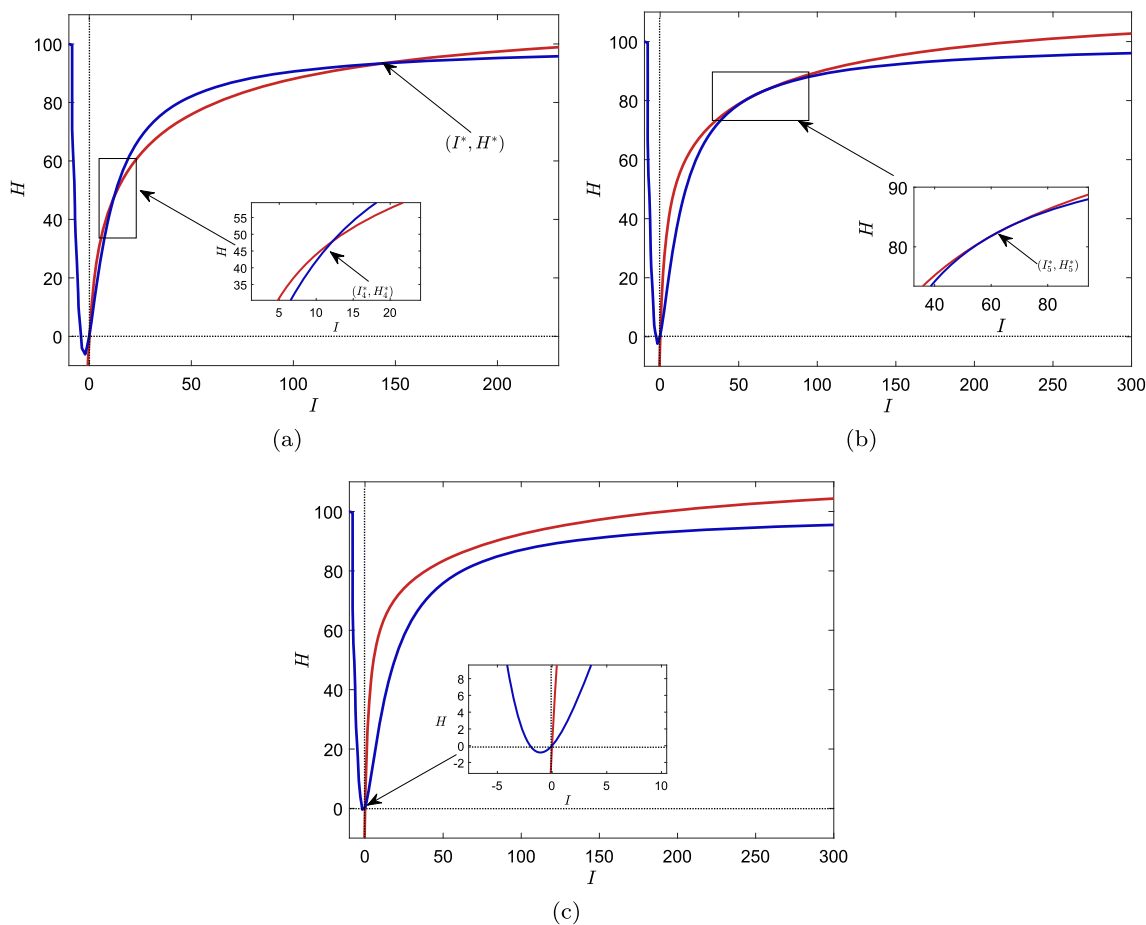
Fig. 3 (**a**–**c**) Intersection scenarios of isoclines (4) and (5) for $R_0 = 1$. Blue curve depicts isocline (4) and red curve depicts isocline (5)

exhibit a crucial behavior,i.e., they tend to converge either towards the stable endemic equilibrium or towards the disease-free equilibrium, contingent upon the initial number of infected individuals.

Biological significance of Figure 9a: The occurrence of saddle-node bifurcation signifies the transition between persistent disease transmission and potential disease elimination. It underscores the importance of targeted interventions to control disease spread and highlights the sensitivity of disease outcomes to initial number of infected individuals when $R_0 \in (0.995, 1)$. Further, the bubbling phenomenon that occurs for $R_0 \in (1.003, 1.06)$ signifies a delicate balance between disease persistence and fluctuations in the infected population. The presence of a stable limit cycle suggests the potential for recurrent outbreaks or oscillations in disease prevalence, underscoring the challenges in disease control and eradication efforts.

The bifurcation diagram plotted in Fig. 9b corresponds to $k_0 = 0.0014$. This figure showcases Hopf bifurcation at $R_0 \approx 1.091$. Once again, this Hopf bifurcation is of a supercritical type. Consequently, stable limit cycles emerge as a consequence of the Hopf point, manifesting in the reverse direction. These limit cycles persist until the value of R_0 reaches approximately 0.995, where they cease to exist due to occurrence of homoclinic bifurcation.

Biological significance of Figure 9b: This figure shows that for $R_0 < 0.995$, the disease will be eliminated from the population, which highlights the importance of maintaining transmission rates below this threshold to prevent outbreaks. In the range $R_0 \in (0.995, 1.091)$, the number of infected individuals fluctuates, which is affected by the amplitude of the limit cycle. This fluctuation underlines the possibility of periodic outbreaks and emphasizes the need for continued surveillance and intervention strategies to manage disease prevalence within manageable limits. Conversely, for $R_0 > 1.091$, the disease will persist within the population, creating challenges for control and mitigation efforts.

Moreover, the bifurcation diagram plotted in Fig. 9c corresponds to $k_0 = 0.0024$. This figure shows that the equilibrium curve exhibits subcritical Hopf bifurcation at $R_0 \approx 1.023$. From this Hopf point, two limit cycles (one stable and one unstable) originate in the forward direction and cease to appear at $R_0 \approx 1.078$ via limit cycle

(a)

(b)

(c)
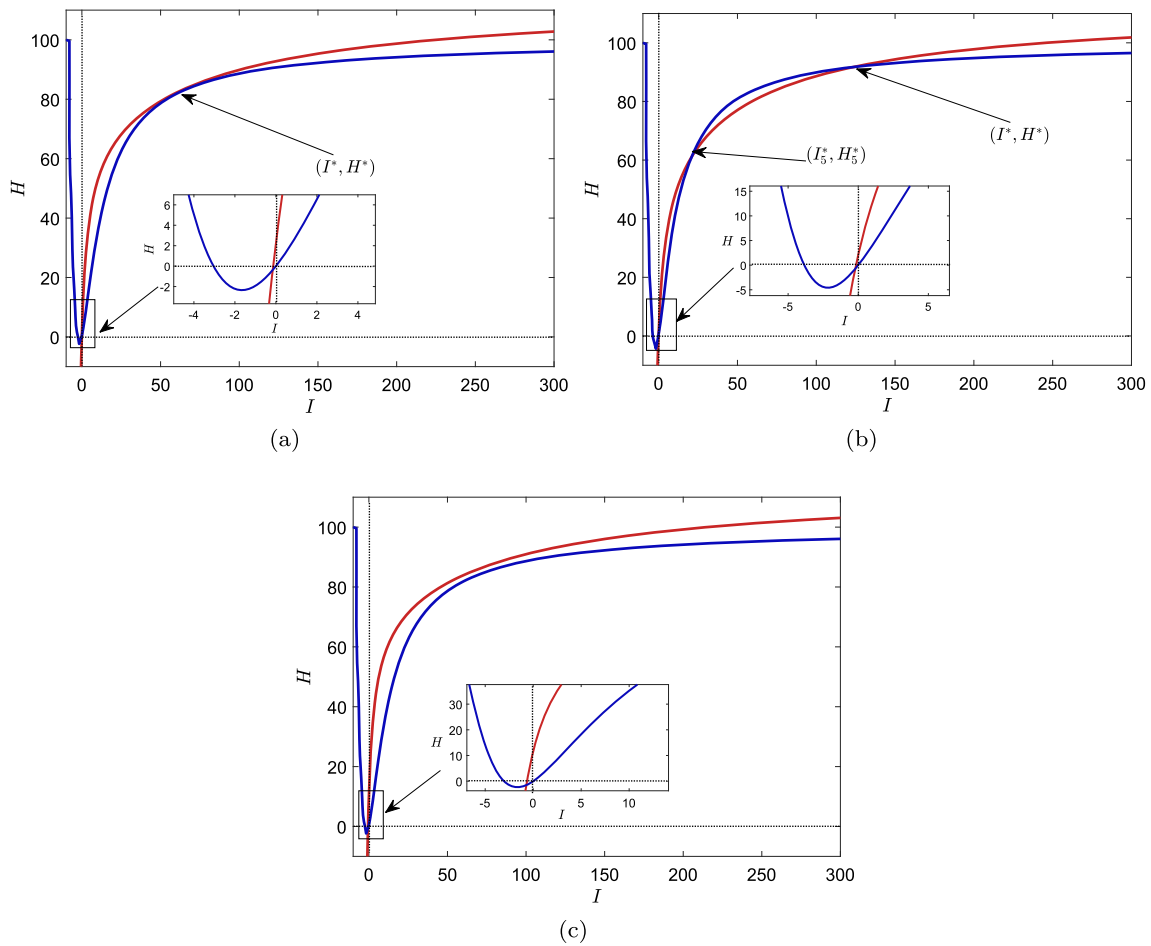
Fig. 4 (**a–c**)Intersection scenarios of isoclines (4) and (5) for $R_0 < 1$. Blue curve depicts isocline (4) and red curve depicts isocline (5)


(a)

(b)
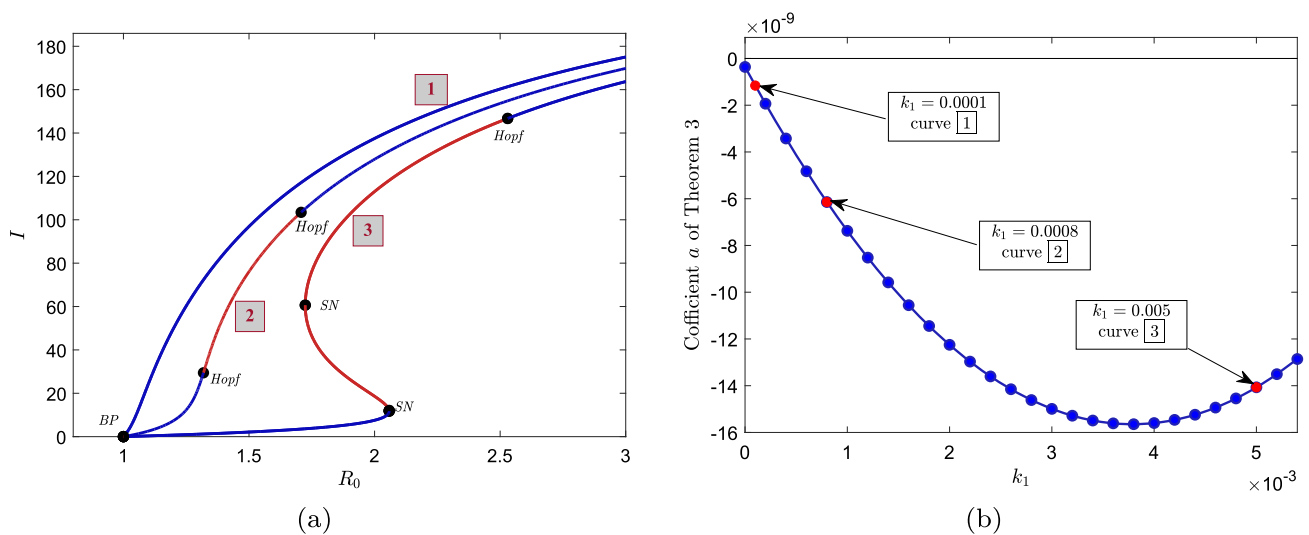
Fig. 5 Equilibrium curves in $R_0 - I$ plane for $k_1 = 0.0001$ (labeled as $\boxed{1}$), $k_1 = 0.0008$ (labeled as $\boxed{2}$) and $k_1 = 0.005$ (labeled as $\boxed{3}$)
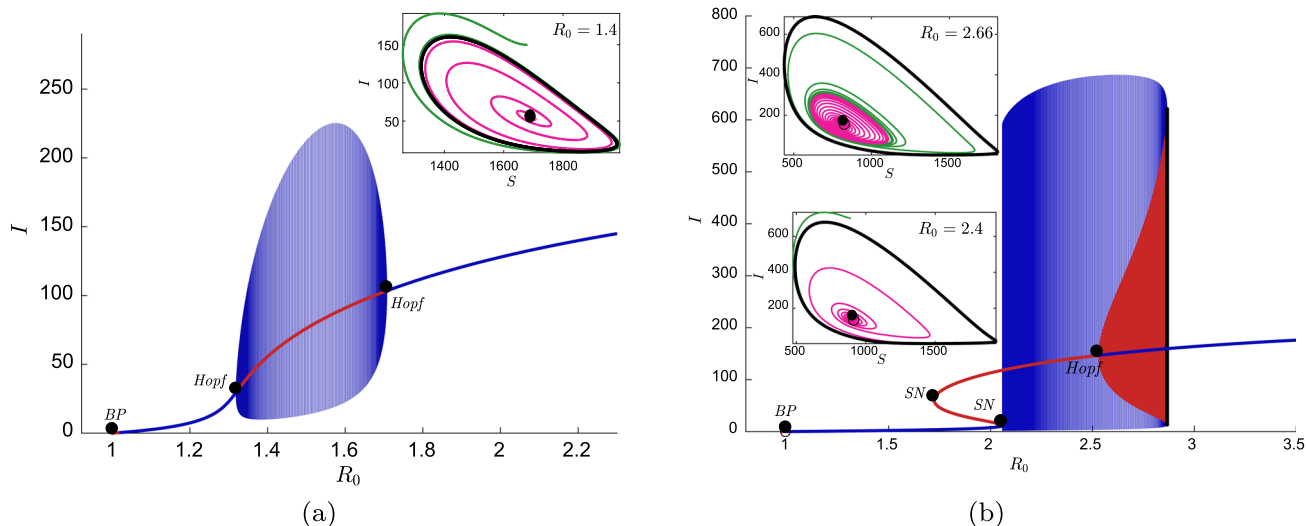
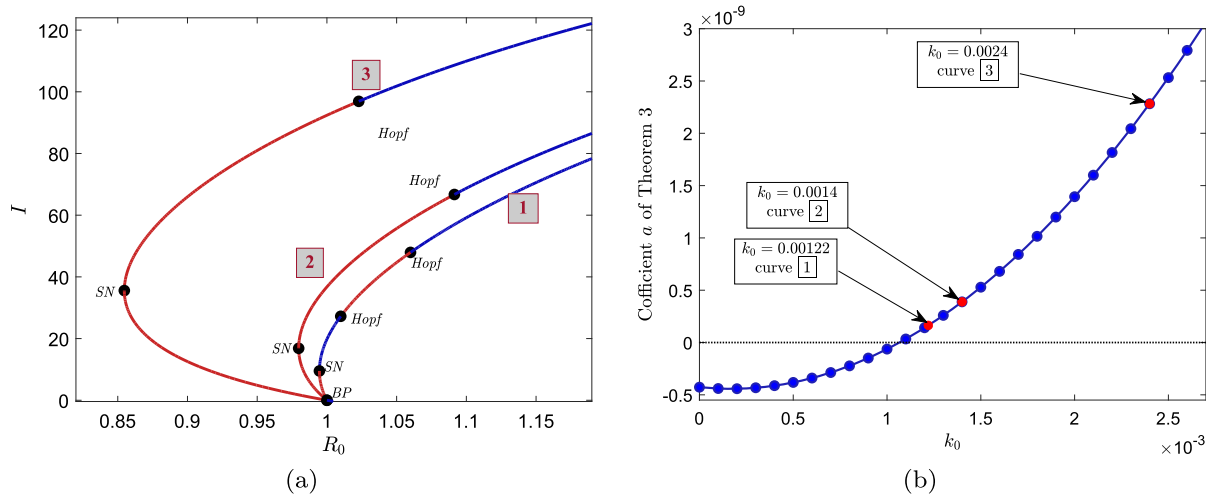**Fig. 6** Bifurcation plot in $R_0 - I$ plane for **a** $k_1 = 0.0008$ **b** $k_1 = 0.005$

Fig. 7 Hopf curve (white curve) and saddle-node curve (black curve) in $R_0 - H_a$ bi-parametric plane. Region I has a single stable endemic equilibrium, Region II features three equilibria (two unstable, one stable), Region III exhibits a stable limit cycle around an unstable endemic equilibrium, and in Region IV, an unstable limit cycle surrounds a stable endemic equilibrium
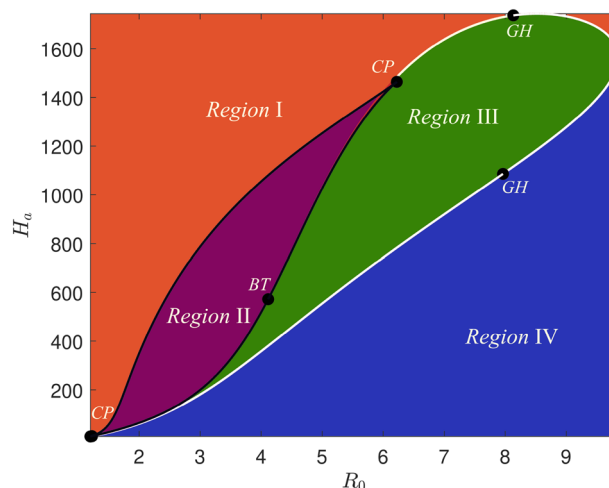

bifurcation. Also, the stable limit cycle originates in the backward direction, disappears at $R_0 \approx 1.001$ through homoclinic bifurcation.

Biological significance of Figure 9c: The depicted figure illustrates critical thresholds in disease dynamics based on the value of the basic reproduction number (R_0). For $R_0 < 1.001$, the disease is likely to be eradicated from the population. However, within the range $R_0 \in (1.001, 1.023)$, the presence of a stable limit cycle leads to fluctuations in the number of infected individuals. This period reflects a delicate balance between disease transmission and control measures, where the amplitude of the limit cycle influences the magnitude of these fluctuations. Subsequently, for $R_0 \in (1.023, 1.078)$, the disease persists within the population, with infected individuals either stabilizing at an equilibrium level or fluctuating based on the amplitude of the stable limit cycle.

We further plot the Hopf curve, saddle-node curve, and homoclinic curve in $R_0 - k_0$ parametric plane for $H_a = 50$, $m = 60$, and $k_1 = 0.0001$ (the remaining parameter values are same as mentioned in Table 1), Fig. 10. These three curves partition the entire plane into four distinct regions and coincide at the 'BT' point. The regions, visually depicted by blue (Region I), pink (Region II), green (Region III), and orange (Region IV) hues. Within these demarcated regions, the dynamical behavior of the model (1) exhibits notable variations. At the BT point $(R_0, k_0) = (0.9825, 0.00137)$ the proposed system has one endemic equilibrium, which is saddle in nature and E_0, which exhibits stability. Thus, all the solution trajectories move toward E_0 as $t \to \infty$. Moreover, within Region I, the model system (1) possesses solely E_0, which is stable. Consequently, when the parameters R_0 and k_0 fall within this region, all solution trajectories converge towards E_0. In Region II, the proposed system features two endemic equilibria, both of which are unstable. Consequently, the solution trajectories gravitate towards E_0. Within Region III, the system exhibits two endemic equilibria, both of which are unstable. However, the endemic

(a)

(b)

Fig. 8 **a** Equilibrium curves in $R_0 - I$ plane for $k_0 = 0.00122$ (labeled as $\boxed{1}$), $k_0 = 0.0014$ (labeled as $\boxed{2}$) and $k_0 = 0.0024$ (labeled as $\boxed{3}$) **b** Plot for coefficient of a of Theorem 3 with respect to k_0

(a)

(b)

(c)
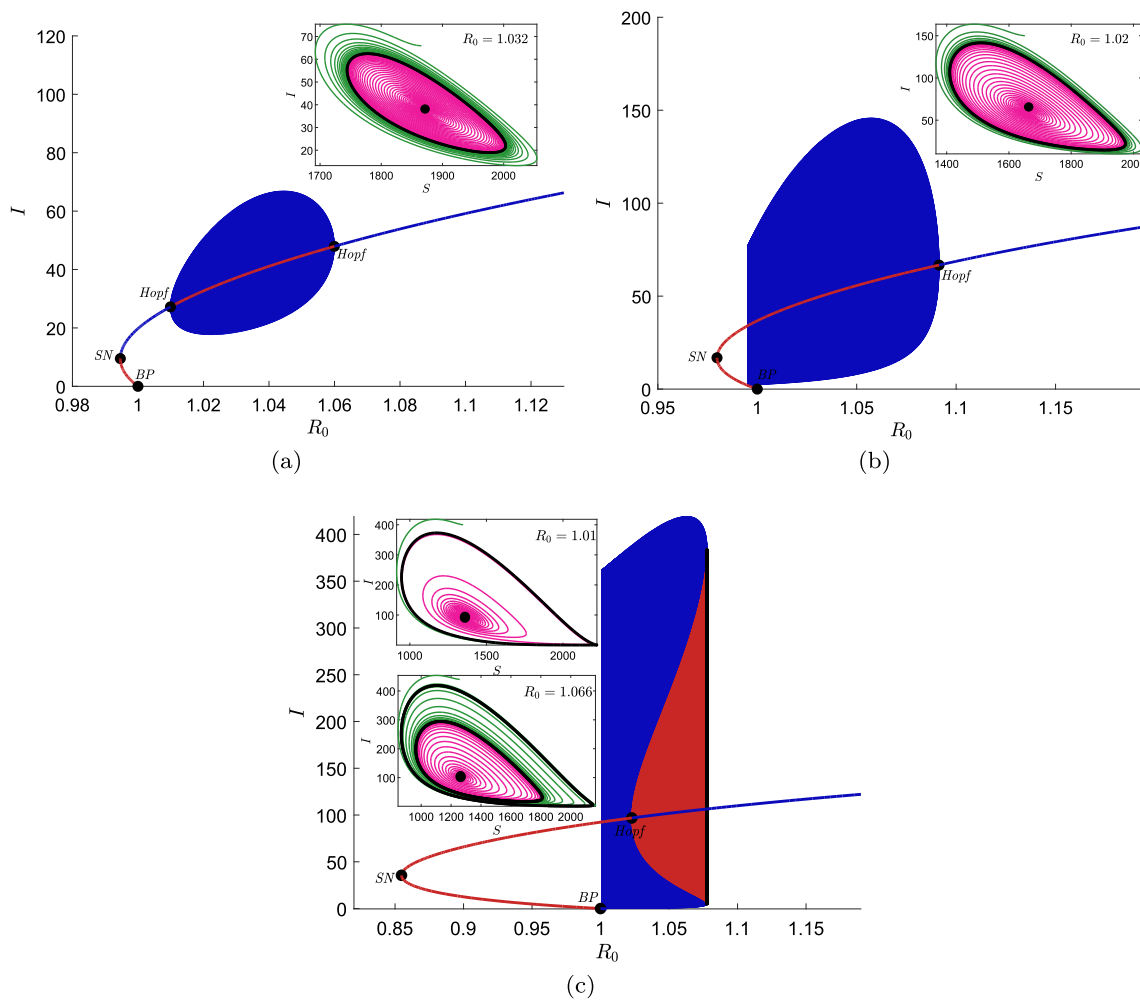
Fig. 9 Bifurcation plot in $R_0 - I$ plane for **a** $k_0 = 0.00122$ **b** $k_0 = 0.0014$ (c) $k_0 = 0.0024$
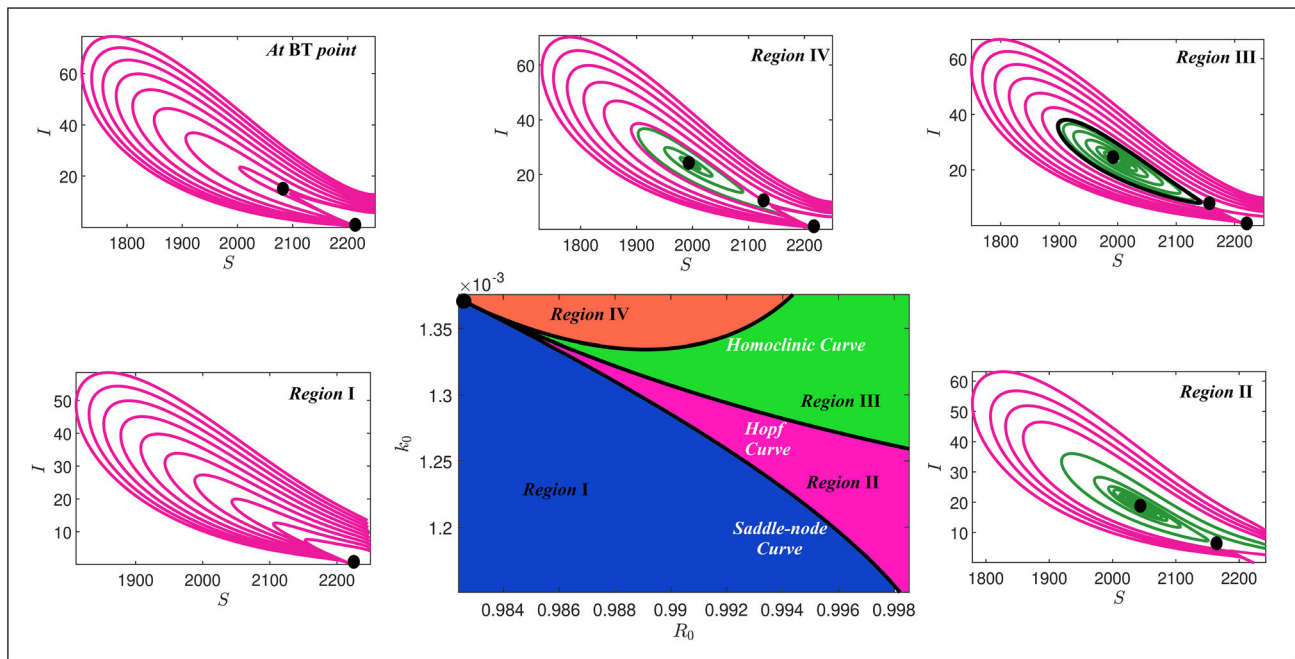
Fig. 10 Unfolding of BT point in $R_0 - k_0$ plane and phase portraits at BT point and corresponding to Region I, II, III, and IV. In Region I, model system (1) only has a stable disease-free equilibrium. In Region II, there are two unstable endemic equilibria. In Region III, there are two unstable endemic equilibria, and a stable limit cycle surrounds the endemic equilibrium with high endemicity. In Region IV, there are two endemic equilibria, one stable and the other unstable

equilibrium associated with higher endemicity is enclosed by a stable limit cycle. As a result, solution trajectories in this region can either gravitate towards E_0 or become attracted to the stable limit cycle. In Region IV, the model system manifests two endemic equilibria. Among them, the equilibrium characterized by high endemicity is stable, while the other is saddle. Therefore, the solution trajectories in this region can either gravitate towards E_0 or stable endemic equilibrium. For a more comprehensive understanding of the dynamics within these regions, Fig. 10 also presents phase portraits corresponding to specific values of R_0 and k_0 at BT point and the value chosen from Regions I, II, III, and IV.

6 Discussion

In the realm of epidemic outbreak control and management, the synergy between healthcare facilities and infrastructure elements, such as robust road networks and efficient ambulance services, stands as an indispensable linchpin. In this research paper, we have presented and examined a mathematical model that highlights the critical role of infrastructure components, in conjunction with healthcare facilities, in efficiently managing an epidemic outbreak. The analysis of the proposed model revealed its susceptibility to a spectrum of bifurcation phenomena. These include the transcritical bifurcation (backward and forward), saddle-node bifurcation, Hopf bifurcation (supercritical and subcritical), and codimension-2 Bogdanov-Takens bifurcation. These findings, while complex in their mathematical expressions, carry profound epidemiological implications. The occurrence of a backward transcritical bifurcation illustrates that the disease can persist within the population even when R_0 is less than one. This occurrence challenges the traditional understanding, indicating that under circumstances where the disease persistence might appear unlikely, specific factors and dynamics come into play, enabling the disease to endure within the population.

Additionally, the numerical simulations also reveal that if the total count of hospital beds within the affected regions remain below a specific critical threshold, the equilibrium level of infected individuals increases, despite well-developed and maintained basic infrastructure. Furthermore, if the healthcare facilities surpass a certain threshold quantity, augmenting logistical infrastructure can indeed result in a reduction of the equilibrium level of infected individuals. Nevertheless, it's imperative to acknowledge that beyond a specific threshold, further enhancement to the logistics infrastructure might have the unintended consequence of complicating the situation rather than improving it. This complication arises due to the occurrence of periodic oscillations via Hopf bifurcation. Thus, if the availability of healthcare facilities in the affected region is less than a threshold quantity, the increase in

infrastructure can destabilize the system, which creates complications for policy makers to cause any decision regarding the control of outbreak.

Future research could delve deeper into the interplay between healthcare infrastructure and epidemic dynamics, particularly focusing on refining the mathematical model to incorporate additional real-world complexities. Investigating the impact of dynamic changes in healthcare capacity, such as seasonal variations or sudden surges in demand, could provide valuable insights into optimal resource allocation strategies during outbreaks. Furthermore, exploring the role of non-pharmaceutical interventions, such as social distancing measures or public awareness campaigns, in conjunction with infrastructure improvements could offer a comprehensive understanding of epidemic control mechanisms.

Data availibility The data substantiating the results of this study can be found within the confines of this article.

Declarations

Conflict of interest There is no Conflict of interest.

References

1. A. Abdelrazec, J. Belair, C. Shan, H. Zhu, Modeling the spread and control of dengue with limited public health resources. Math. Biosci. **271**, 136–145 (2016). https://doi.org/10.1016/j.mbs.2015.11.004
2. G.O. Agaba, Y.N. Kyrychko, K.B. Blyuss, Mathematical model for the impact of awareness on the dynamics of infectious diseases. Math. Biosci. **286**, 22–30 (2017). https://doi.org/10.1016/j.mbs.2017.01.009
3. M. Aguiar, N. Stollenwerk, B.W. Kooi, Modeling infectious diseases dynamics: Dengue fever, a case study, *In Epidemiology Insights* IntechOpen (2012)
4. A. Ajbar, R.T. Alqahtani, M. Boumaza, Dynamics of a COVID-19 model with a nonlinear incidence rate, quarantine, media effects, and number of hospital beds. Symmetry **13**(947), 1–14 (2021). https://doi.org/10.3390/sym13060947
5. F. Al Basir, S. Ray, E. Venturino, Role of media coverage and delay in controlling infectious diseases: a mathematical model. Appl. Math. Comput. **337**, 372–385 (2018). https://doi.org/10.1016/j.amc.2018.05.042
6. M.E. Alexander, S.M. Moghadas, Periodicity in an epidemic model with a generalized non-linear incidence. Math. Biosci. **189**, 75–96 (2004). https://doi.org/10.1016/j.mbs.2004.01.003
7. H.J. Alsakaji, S. Kundu, F.A. Rihan, Delay differential model of one-predator two-prey system with Monod-Haldane and holling type II functional responses. Appl. Math. Comput. **397**, 125919 (2021). https://doi.org/10.1016/j.amc.2020.125919
8. J. Barado, J.M. Guergue, L. Esparza, C. Azcarate, F. Mallor, S. Ochoa, A mathematical model for simulating daily bed occupancy in an intensive care unit. Crit. Care Med. **40**, 1098–1104 (2012). https://doi.org/10.1097/CCM.0b013e3182374828
9. C. Barril, P.A. Bliman, S. Cuadrado, Final size for epidemic models with asymptomatic transmission. Bull. Math. Biol. **85**, 52 (2023). https://doi.org/10.1007/s11538-023-01159-y
10. H. Bilgil, A. Yousef, A. Erciyes, U. Erdinç, Z. Ozturk, A fractional-order mathematical model based on vaccinated and infected compartments of SARS-CoV-2 with a real case study during the last stages of the epidemiological event. J. Comput. Appl. Math. **425**, 115015 (2023). https://doi.org/10.1016/j.cam.2022.115015
11. S. Cakan, Dynamic analysis of a mathematical model with health care capacity for COVID-19 pandemic. Chaos. Solit. Fractals **139**, 110033 (2020). https://doi.org/10.1016/j.chaos.2020.110033
12. C. Castillo-Chavez, B. Song, Dynamical models of tuberculosis and their applications. Math. Biosci. Eng. **1**, 361–404 (2004). https://doi.org/10.3934/mbe.2004.1.361
13. Y. Chen, Y. Yang, W. Peng, H. Wang, Influence and analysis of ambulance on the containment of COVID-19 in China. Saf. Sci. **139**, 105160 (2021). https://doi.org/10.1016/j.ssci.2021.105160
14. C.T. Codec, Endemic and epidemic dynamics of cholera: the role of the aquatic reservoir. BMC Infect. Dis. **1**, 1–14 (2001). https://doi.org/10.1186/1471-2334-1-1
15. J. Cui, Y. Sun, H. Zhu, The impact of media on the control of infectious diseases. J. Dyn. Diff. Equat. **20**, 31–53 (2008). https://doi.org/10.1007/s10884-007-9075-0
16. S.D. Djiomba Njankou, F. Nyabadza, Modelling the potential impact of limited hospital beds on Ebola virus disease dynamics. Math. Methods Appl. Sci. **41**, 8528–8544 (2018). https://doi.org/10.1002/mma.4789
17. S. Feng, J. Zhang, J. Li, X.F. Luo, H. Zhu, M.Y. Li, Z. Jin, The impact of quarantine and medical resources on the control of COVID-19 in Wuhan based on a household model. Bull. Math. Biol. **84**, 47 (2022). https://doi.org/10.1007/s11538-021-00989-y

18. J.K. Ghosh, S.K. Biswas, S. Sarkar, U. Ghosh, Mathematical modelling of COVID-19: a case study of Italy. Math. Comput. Simul. **194**, 1–18 (2022). https://doi.org/10.1016/j.matcom.2021.11.008

19. J. Guo, F. Huang, J. Liu, Y. Chen, W. Wang, B. Cao, Z. Zou, S. Liu, J. Pan, C. Bao, M. Zeng, H. Xiao, H. Gao, S. Yang, Y. Zhao, Q. Liu, H. Zhou, J. Zhu, X. Liu, W. Liang, Y. Yang, S. Zheng, J. Yang, H. Diao, K. Su, L. Shao, H. Cao, Y. Wu, M. Zhao, S. Tan, H. Li, X. Xu, C. Wang, J. Zhang, L. Wang, J. Wang, J. Xu, D. Li, N. Zhong, X. Cao, G.F. Gao, L. Li, C. Jiang, The serum profile of hypercytokinemia factors identified in H7N9-infected patients can predict fatal outcomes. Sci. Rep. **6**, 21230 (2016). https://doi.org/10.1038/srep21230

20. M.E. Halloran, I.M. Longini, A. Nizam, Y. Yang, Containing bioterrorist smallpox. Science **298**, 1428–1432 (2002)

21. E. Hammarlund, M.W. Lewis, S.G. Hansen, L.I. Strelow, J.A. Nelson, G.J. Sexton, J.M. Hanifin, M.K. Slifka, Duration of antiviral immunity after smallpox vaccination. Nat. Med. **9**, 1131–1137 (2003). https://doi.org/10.1038/nm917

22. B.F. Haynes, G. Pantaleo, A.S. Fauci, Toward an understanding of the correlates of protective immunity to HIV infection. Science **271**, 324–328 (1996)

23. H.W. Hethcote, The mathematics of infectious diseases. SIAM Rev. (2000). https://doi.org/10.1137/S0036144500371907

24. M.J. Keeling, C.A. Gilligan, Metapopulation dynamics of bubonic plague. Nature **407**, 903–906 (2000). https://doi.org/10.1038/35038073

25. A. Kumar, A. Gupta, U.S. Dubey, B. Dubey, Stability and bifurcation analysis of an infectious disease model with different optimal control strategies. Math. Comput. Simul. **213**, 78–114 (2023). https://doi.org/10.1016/j.matcom.2023.05.024

26. S. Kundu, H.J. Alsakaji, F.A. Rihan, S. Maitra, R.K. Upadhyay, Investigating the dynamics of a delayed stage-structured epidemic model with saturated incidence and treatment functions. Eur. Phys. J. Plus **137**(1), 171 (2022). https://doi.org/10.1140/epjp/s13360-022-02351-0

27. R. Liu, J. Wu, H. Zhu, Media/psychological impact on multiple outbreaks of emerging infectious diseases. Comput. Math. Methods Med. **8**(3), 153–164 (2007). https://doi.org/10.1080/17486700701425870

28. L. Lu, M. Jia, Y. Ma, L. Yang, Z. Chen, D.D. Ho, Y. Jiang, L. Zhang, The changing face of HIV in China. Nature **455**, 609 (2008). https://doi.org/10.1038/455609a

29. X. Meng, S. Zhao, T. Feng, T. Zhang, Dynamics of a novel nonlinear stochastic SIS epidemic model with double epidemic hypothesis. J. Math. Anal. Appl. **433**(1), 227–242 (2016). https://doi.org/10.1016/j.jmaa.2015.07.056

30. J. Meade, A mathematical model for deriving hospital service areas. Int. J. Health Serv. **4**, 353–364 (1974)

31. A.K. Misra, J. Maurya, Allocation of hospital beds on the emergence of new infectious disease: a mathematical model. Chaos: Interdiscip. J. Nonlinear Sci. **33**, 043125 (2023). https://doi.org/10.1063/5.0133703

32. A.K. Misra, J. Maurya, M. Sajid, Modeling the effect of time delay in the increment of number of hospital beds to control an infectious disease. Math. Biosci. Eng. **19**, 11628–11656 (2022). https://doi.org/10.3934/mbe.2022541

33. A.K. Misra, J. Maurya, Bifurcation analysis and optimal control of an epidemic model with limited number of hospital beds. Int. J. Biomath. **16**, 2250101 (2023). https://doi.org/10.1142/S1793524522501017

34. A.K. Misra, J. Maurya, Modeling the importance of temporary hospital beds on the dynamics of emerged infectious disease. Chaos: Interdiscip. J. Nonlinear Sci. **31**, 103125 (2021). https://doi.org/10.1063/5.0064732

35. J. Maurya, K.B. Blyuss, A.K. Misra, Modeling the impact of hospital beds and vaccination on the dynamics of an infectious disease. Math. Biosci. **368**, 109133 (2024). https://doi.org/10.1016/j.mbs.2023.109133

36. National Academies of Sciences, *Engineering, and Medicine* (Moving upstream to improve the nation's health, Integrating social care into the delivery of health care, 2019)

37. J. Pang, J.A. Cui, J. Hui, Rich dynamics of epidemic model with sub-optimal immunity and nonlinear recovery rate. Math. Comput. Model. **54**, 440–448 (2011). https://doi.org/10.1016/j.mcm.2011.02.033

38. L. Perko, *Differential equations and dynamical systems*. Springer Science & Business Media 7 (2013)

39. F.A. Rihan, H.J. Alsakaji, C. Rajivganthi, Stochastic SIRC epidemic model with time-delay for COVID-19. Adv. Differ. Equ. **2020**(1), 502 (2020). https://doi.org/10.1186/s13662-020-02964-8

40. S. Samanta, Study of an epidemic model with Z-type control. Int. J. Biomath. **11**, 1850084 (2018)

41. C. Shan, H. Zhu, Bifurcations and complex dynamics of an SIR model with the impact of the number of hospital beds. J. Differ. Equ. **257**, 1662–1688 (2014). https://doi.org/10.1016/j.jde.2014.05.030

42. Q. Sun, T. Miyoshi, S. Richard, Analysis of COVID-19 in Japan with extended SEIR model and ensemble Kalman filter. J. Comput. Appl. Math. **419**, 114772 (2023). https://doi.org/10.1016/j.cam.2022.114772

43. P. Tamilalagan, B. Krithika, P. Manivannan, S. Karthiga, Is reinfection negligible effect in COVID-19? A mathematical study on the effects of reinfection in COVID-19. Math. Methods Appl. Sci. **46**(18), 19115–19134 (2023). https://doi.org/10.1002/mma.9614

44. J.A. Tenreiro Machado, J. Ma, Nonlinear dynamics of COVID-19 pandemic: modeling, control, and future perspectives. Nonlinear Dyn. **101**, 1525–1526 (2020). https://doi.org/10.1007/s11071-020-05919-6

45. P. Van den Driessche, J. Watmough, Reproduction numbers and sub-threshold endemic equilibria for compartmental models of disease transmission. Math. Biosci. **180**, 29–48 (2002). https://doi.org/10.1016/S0025-5564(02)00108-6

46. A. Wang, Y. Xiao, H. Zhu, Dynamics of a Filippov epidemic model with limited hospital beds. Math. Biosci. Eng. **15**, 739 (2018). https://doi.org/10.3934/mbe.2018033

47. Y. Xu, L. Wei, X. Jiang, Z. Zhu, Complex dynamics of a SIRS epidemic model with the influence of hospital bed number. Discret. Contin. Dyn. Syst. Ser. B. **26**, 6229–6252 (2021). https://doi.org/10.3934/dcdsb.2021016

48. L. Zhou, M. Fan, Dynamics of an SIR epidemic model with limited medical resources revisited. Nonlinear Anal. Real World Appl. **13**(1), 312–324 (2012). https://doi.org/10.1016/j.nonrwa.2011.07.036